Electronic Supplementary Material (ESI) for Journal of Materials Chemistry C.

"Supporting Information"

Large electroresistance and tunable photovoltage of ferroelectric nanocapacitors based on ultrathin super-tetragonal $BiFeO_3$

Hua Fan,[1] Zhen Fan,[1] Peilian Li,[1] Fengyuan Zhang,[1] Guo Tian,[1] Junxiang Yao,[1] Zhongwen Li,[1] Xiao Song,[1] Bing Han,[1] Deyang Chen,[1] Min Zeng,[1] Sujuan Wu,[1] Zhang Zhang,[1] Minghui Qin,[1] Xubing Lu,[1] Zhi Zhang,[2] Jiyan Dai,[2] Zengxing Lu,[3] Xingsen Gao,[1] and Junming Liu[3*]*

[1]*Institute for Advanced Materials and Guangdong Provincial Key Laboratory of Quantum Engineering and Quantum Materials, South China Normal University, Guangzhou 510006, China*

[2]*Department of Applied Physics, Hong Kong Polytechnic University, Hong Kong, China*

[3]*Laboratory of Solid State Microstructures, Nanjing University, 210093, China*

***** Email: xingsengao@scnu.edu.cn, liujm@nju.edu.cn

PS mask fabrication process. First, a commercial water solution of polystyrene spheres (PS, 2.5 wt%, diameter = 500 nm) diluted 1:1 by volume with alcohol, was added into distilled water, to get a monolayer of closely arranged PS on the top surface of the distilled water. Then, the BFO film was immersed into the solution. Next, the BFO film together with a mono layer of PS was extracted and dried at room temperature. After that, the top electrodes (Au) were deposited by thermal evaporation. Finally, the PS template was dissolved by analytical reagent chloroform and the ordered nanoelectrode arrays were obtained.

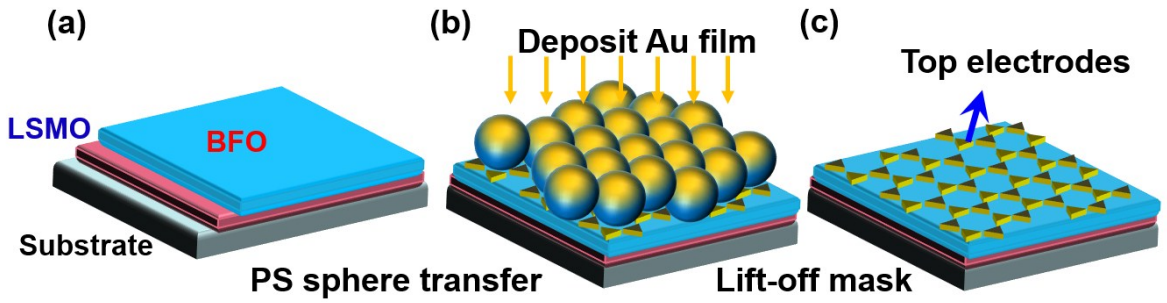

Figure S1. Schematic for the fabrication of well-ordered array of top nanoelectrodes.

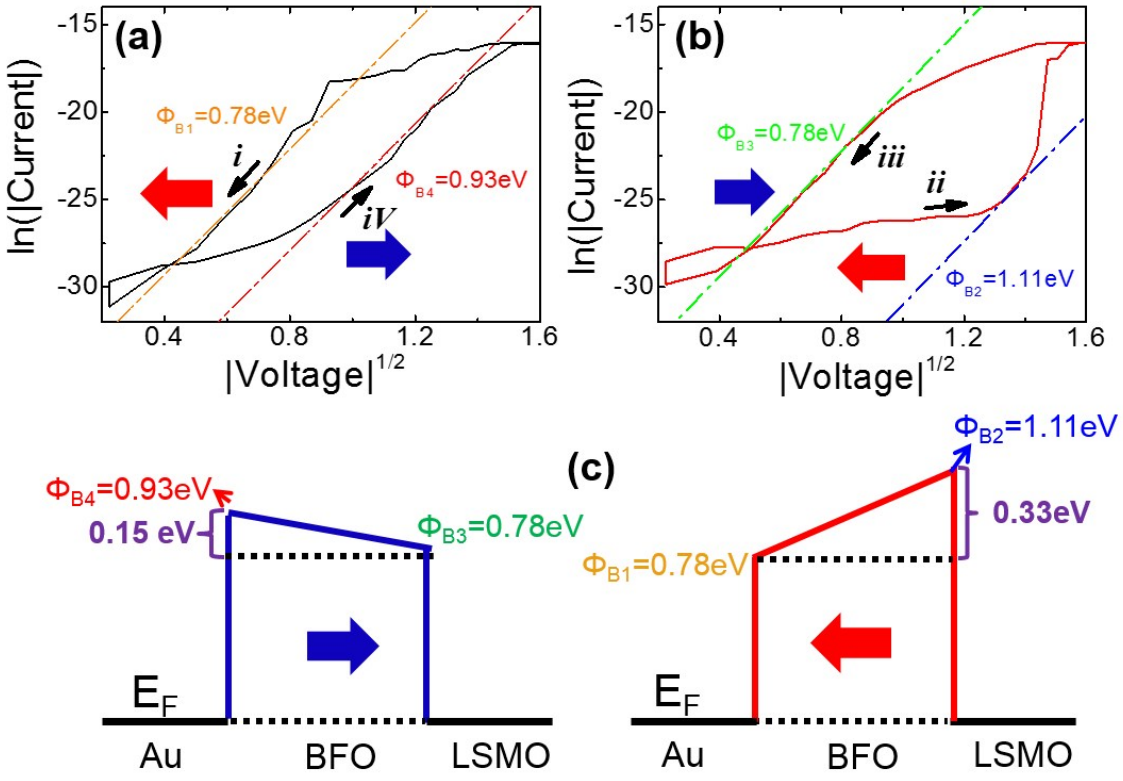

Figure S2. Interface band structure of Au/T-BFO (8nm)/LSMO capacitors at dark：(a,b) *I-V* curves plotted as ln |Current| vs |Voltage|$^{1/2}$ for negative bias voltages (a) and positive bias voltages (b). (c) Interface energy profiles of the heterostructure in two opposite polarization states derived from the above fitting: downward (left) and upward (right) states.

We have used the Schottky emission equation for the fitting of *I-V* curves:

$$I = AA^{**}T^2 \exp\left(\frac{-\Phi_B + \sqrt{\frac{q^3 E}{4\pi\varepsilon_0\varepsilon_f}}}{k_B T}\right) \quad (1)$$

where Φ_B the Schottky barrier, and A is the electrode area, A^{**} the effective Richardson constant, T is the Kelvin temperature, q is the electron charge, ε_0 is the vacuum permittivity, ε_f is the image force lowering permittivity (slightly larger than the optical permittivity ε_{opt}), and k_B is the Boltzmann constant.

For the *I-V* curve *i*, the polarization is in the P_{down} state and the Au/T-BFO barrier is blocking the current flow. Therefore, through fitting the *I-V* curve *i* to Eq. (1), the barrier height Φ_{B1} can be extracted. Using the same way, the barrier heights Φ_{B2}, Φ_{B3}, and Φ_{B4} can also be obtained. The asymmetric modulations of polarization on the barrier heights may be due to the different dielectric constants and/or screening lengths of the metal electrodes. The effect of P on Φ_B can be described as (Pantel et al., Phys. Rev. B 82, 134105 (2010)):

$$\Delta\Phi_{Bi} = \frac{l_i Q_S}{\varepsilon_0 \varepsilon_{Mi}} q, i = 1, 2, \tag{2}$$

and,

$$Q_S = \frac{Pd}{\varepsilon_{stat}\left(\frac{l_1}{\varepsilon_{M1}} + \frac{l_2}{\varepsilon_{M2}}\right) + d} \tag{3}$$

where $\Delta\Phi_{Bi}$ is the barrier height variation due to the imperfect screening of polarization, Q_S is the screening charge, l_i is the screening length and ε_{Mi} is the dielectric constant of the metal electrode. As can be seen From Eq. (2) and (3), the variable parameters that determine the $\Delta\Phi_{Bi}$ are the l_i and ε_{Mi}. Because the two electrodes are different, i.e., Au and LSMO, the variations of barrier heights at the two interfaces can also be different.

According to Eq. (1)-(3) in this letter, a large P_r leads to a large modulation on the barrier height $\Delta\Phi_{Bi}$, which is beneficial for both the electroresistance ratio and the photovoltage. This is supported by our observation that large on/off ratio in T-BFO than R-BFO with the same thickness, which also agrees with previous reports.

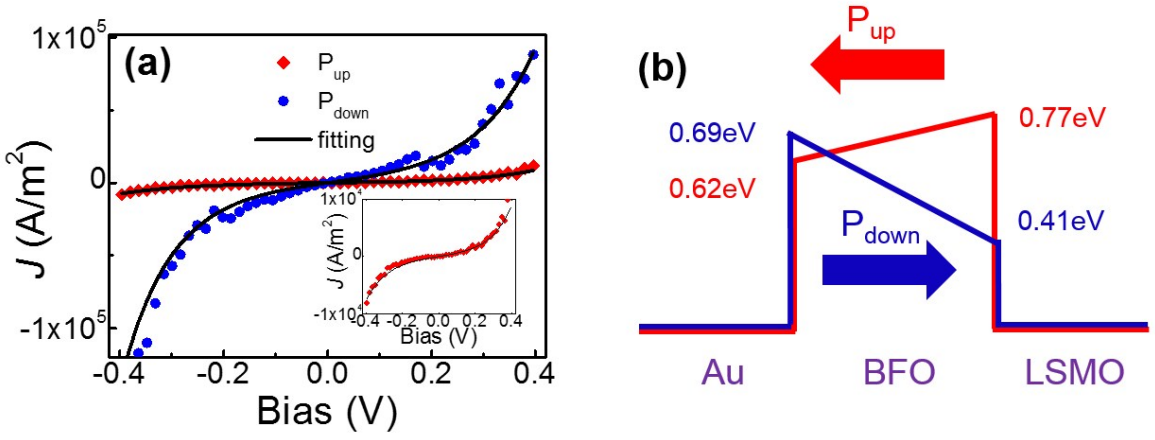

Figure S3. (a) Fitting of the *I-V* curves for the 2.5-nm film using the tunneling model. (b) Schematic potential energy profiles of the Au/BFO (2.5 nm)/LSMO heterostructure in different polarization states.

The tunneling model given by Gruverman et al. (Nano Lett. 9, 3539-3543 (2009)) is used to simulate the *I-V* curves of the 2.5-nm film:

$$J \cong C\frac{\exp\left\{\alpha(V)\left[\left(\Phi_2-\frac{eV}{2}\right)^{3/2}-\left(\Phi_1+\frac{eV}{2}\right)^{3/2}\right]\right\}}{\alpha^2(V)\left[\left(\Phi_2-\frac{eV}{2}\right)^{1/2}-\left(\Phi_1+\frac{eV}{2}\right)^{1/2}\right]^2}\times\sinh\left\{\frac{3}{2}\alpha(V)\left[\left(\Phi_2-\frac{eV}{2}\right)^{1/2}-\left(\Phi_1+\frac{eV}{2}\right)^{1/2}\right]\frac{eV}{2}\right\}, \quad (4)$$

where $C=-(4em)/(9\pi^2\mathrm{h}^3)$, (5)

and $\alpha(V)\equiv\left[4d(2m)^{1/2}\right]/\left[3\mathrm{h}(\Phi_1+eV-\Phi_2)\right]$. (6)

In Eqs. (4)-(6), Φ_2 and Φ_1 are the potential barriers at the Au/BFO and BFO/LSMO interfaces, respectively, *m* is the effective tunneling mass and *d* is the barrier thickness. As clearly seen in Figure S5, the tunneling model can fit the *I-V* data of the 2.5-nm film fairly well.

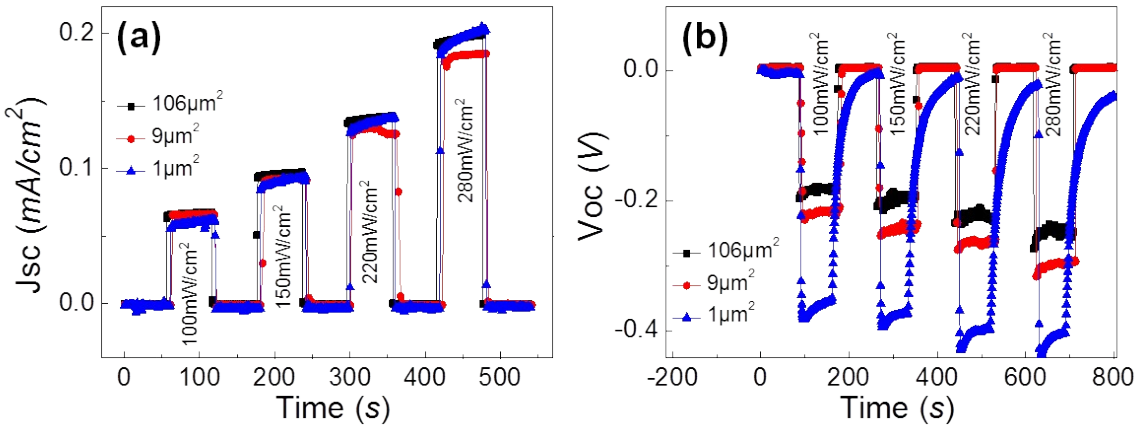

Figure S4. Photovoltaic properties for the Au/T-BFO (8nm)/LSMO capacitors with various lateral sizes: (a) Open-circuit voltage V_{oc} and (b) short-circuit current density J_{sc}. The light was turned on and off alternatively during the measurement.

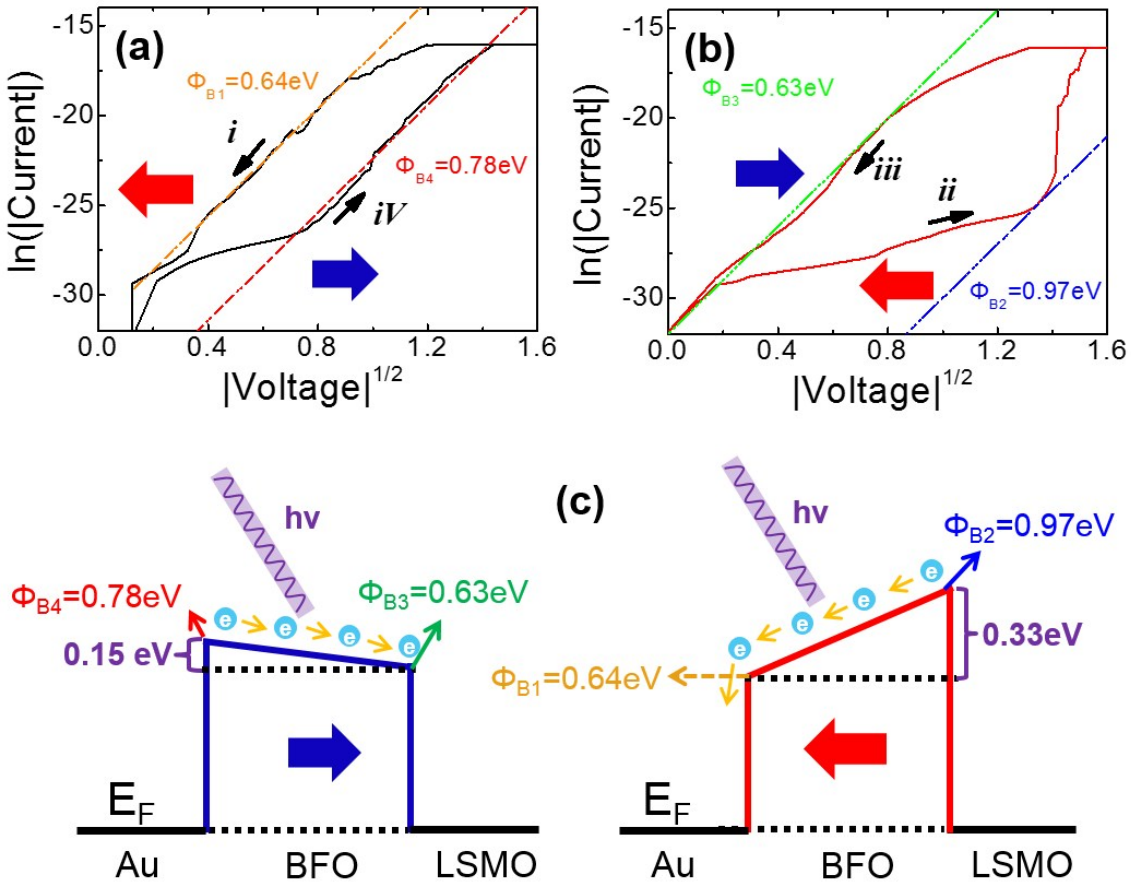

Figure S5. Interface band structure of Au/T-BFO (8nm)/LSMO capacitors under light illumination：(a,b) *I-V* curves plotted as ln |Current| vs |Voltage|$^{1/2}$ for negative bias voltages (a) and positive bias voltages (b). (c) Interface energy profiles of the heterostructure in two opposite polarization states derived from the above fitting: downward (left) and upward (right) states.